ON THE EXTRACTION OF HIGH ENERGY PARTICLE

INFORMATION FROM COSMIC RAY EMULSION DATA*

P. M. Fishbane and J. S. Trefil
University of Virginia
Charlottesville, Virginia 22901

J. L. Newmeyer
Stanford Linear Accelerator Center
Stanford University, Stanford, California 94305

ABSTRACT

The use of data from cosmic ray interactions with dense targets is discussed from the point of view of extracting information on p-p interactions at high (cosmic ray) energies. We present a result which relates single particle inclusive distributions on nuclear targets to single particle inclusive distributions on nucleons. We show that there exists no serious conflict between present nuclear data and a flat pionization region.

(Submitted to Phys. Rev.)

I. INTRODUCTION

A great deal of experimental and theoretical effort in high energy physics today is directed towards single-particle inclusive density functions

$$\rho_c \equiv \frac{1}{\sigma_{ab}^{tot}} E_c \frac{d^3\sigma_{ab \to c}}{d^3 p_c} \tag{1.1}$$

for the inclusive experiment $a + b \to c + $ anything. This function is normalized such that

$$\int \left(\frac{d^3 p_c}{E_c} \right) \rho_c = \langle n_c \rangle , \tag{1.2}$$

the average number of particles of type c produced.

Ideas on scaling[1] have greatly clarified our understanding of ρ_c as the invariant energy variable $s \to \infty$. It is the statement of Feynman scaling that in this limit the differential inclusive cross section can be expressed in terms of just two variables,

$$d\sigma_{ab \to c} = \frac{d^3 p_c}{E_c} f_c(p_\parallel , q, s) \xrightarrow[s \to \infty]{} d^2 q \frac{dx}{x} f_c(x, q) , \tag{1.3}$$

where q is the transverse momentum of particle c, and $x = 2 p_{c,\parallel}^{(cm)} / \sqrt{s}$.

In many respects scaling ideas are more conveniently expressed in terms of the rapidity r defined by

$$\sinh r = \frac{p_\parallel}{\sqrt{q^2 + m^2}} \quad \longleftrightarrow \quad \sinh r^{(CM)} = \frac{x\sqrt{s}}{2\sqrt{q^2 + m^2}} \tag{1.4}$$

In particular, the rapidity is simply additive under Lorentz boosts in the longitudinal direction. Thus, for example, for particle c,

$$r_c^{(CM)} = r_c^{(LAB)} - \sinh^{-1} \frac{p_a^{(CM)}}{m_a} \qquad (1.5)$$

In terms of this variable the single particle invariant phase space can be written as

$$\frac{d^3p}{E} = d^2q \, dr \qquad (1.6)$$

Consequently,

$$\int \rho_c \, d^2q = \frac{dn_c}{dr} \qquad (1.7)$$

where dn_c is the differential change in multiplicity of particles of type c over a range dr in rapidity. Due to the experimental presence of a cut-off in q, the integral converges rapidly.

Theoretical arguments have been presented which state that it is interesting to split the function dn/dr into three regions, according to whether r is "near" the projectile or target rapidity (projectile or target fragmentation region), or in a large region in between whose width in r-space grows like $\ln(s)$ (pionization region). It has been further hypothesized that dn/dr will be flat in the pionization region, giving rise to an overall multiplicity which grows like $\ln(s)$. Thus we are led to expect a single-particle inclusive distribution dn/dr for the reaction, say, $\pi + p \rightarrow \pi + X$, of the (schematic) form shown in Figure 1a as a function of r_c measured in the lab frame.

In view of the fact that relevant features of this central region reveal themselves only on a logarithmic energy scale, it is clearly useful to study

energies which are currently attained only in cosmic rays. Since the flux of primary cosmic rays falls rapidly with increasing energy (flux $\propto$ (E/GeV)$^{-1.7}$), dense materials (such as nuclear emulsions) are very attractive as experimental targets.

We therefore want to be able to extract information on a hadronic process such as $\pi + p \rightarrow \pi + X$ (referred to as I below) at very high energies in terms of the experimentally more accessible information on a nuclear process such as $\pi + A \rightarrow \pi + X$ (referred to as II below). Our purpose in this paper will be to discuss dn_c/dr as a function of lab rapidity for II in terms of the corresponding function for the reaction I. The reason this is not a trivial procedure is the possibility that an intranuclear cascade (see Figure 2) can develop.

The remainder of this paper will be concerned with deriving the formalism that relates reactions I and II, and then applying the formalism to current cosmic ray data at several tens of TeV. The approach to the problem will actually be inverse to the problem itself: that is, we shall ask, "What form should we expect for reaction II when we have a particular (known) form for reaction I?"

The derivation breaks into two parts. In the first part, considered in Section II, we develop a procedure for writing down any general cascade diagram (as in Figure 2) and determining its contribution to the total dn/dr; in the second part (Section III) we incorporate the nuclear physics into the procedure.

Section IV is devoted to applications of the formalism finally written down in Section III. Working with an idealized high energy multiperipheral form for reaction I, we obtain a prediction for the multiplicity $\langle n_c \rangle$ and differential multiplicity dn_c/dr vs. r for reaction II on a typical emulsion nucleon for energies in the TeV range. We find in fact that a flat pionization

region in reaction I leads in general to a rather rapid buildup of multiplicity at the lower rapidities (lab frame) simply because any particle in a cascade can only produce particles of energy less than itself. It is seen that recent experimental results are in excellent quantitative agreement with a flat pionization region for reaction I.

In Section V we present conclusions and caveats. This paper fills in the details of results previously presented in Phys. Rev. Letters.[2] We refer the reader there for further discussion.

II. DIAGRAMS

A. Contributions of Individual Diagrams

We consider first the contribution of the simplest (most basic) diagram, Figure 3a. In this diagram we have an incident pion (rapidity $r = \phi$) making an inelastic collision with a nucleon, resulting in a shower of pions. To maintain complete generality in the discussion, we shall represent the distribution for these "first generation" pions by

$$\frac{dn}{dr_1} = h_1(\phi, r_1) \qquad (2.1)$$

i.e., as a function of only the incident pion's rapidity ϕ (which is related to s) and the observed pion's rapidity r_1. (The arguments here and in all the following will be most transparent in the target rest frame, i.e., lab frame.)

It is convenient also to define

$$\nu_1 = \int h_1(\phi, r_1)\, dr_1 \qquad (2.2)$$

where $\nu_1 \equiv \nu_1(\phi)$ is the multiplicity of first generation pions in a single inelastic collision.

Now let us consider the next simplest diagram, that shown in Figure 3b. This diagram represents the same process as figure 3a (an incident pion of rapidity ϕ making a first generation) except that one of the first generation pions has itself undergone an inelastic collision on another nucleon, making a "second generation" of pions indicated by the dashed circle. (We label the "generation" of a particle as the number of inelastic collisions by which it is removed from the primary projectile.) If the first generation pion which fathered these happened to have a particular rapidity r_1', then the distribution dn/dr_2 of the pions in the dashed circle is $dn/dr_2 = h_1(r_1', r_2)$. But since different values for r_1' for the father occur with frequencies given by the first generation distribution $dn/dr_1 = h_1(\phi, r_1)$ — i.e., since any pion in the first generation is equally likely to be the father of this second generation — it is really more meaningful to speak of an average distribution $\left\langle \dfrac{dn}{dr_2} \right\rangle$ of the pions in the dashed circle. By definition of average, this is just

$$\left\langle \frac{dn}{dr_2} \right\rangle = \frac{\int h_1(\phi, r_1') \, h_1(r_1', r_2) \, dr_1'}{\int h_1(\phi, r_1') \, dr_1' \equiv \nu_1} \equiv h_2(\phi, r_2) \qquad (2.3$$

and we can define

$$\nu_2 = h_2(\phi, r_2) \, dr_2 \qquad (2.4)$$

as the mean multiplicity of pions in a single second generation.

Thus the net average distribution $\left\langle \dfrac{dn}{dr} \right\rangle$ for the entire diagram of Figure 3b — including the first generation in that graph — is just

$$\left\langle \frac{dn}{dr} \right\rangle = \frac{\nu_1 - 1}{\nu_1} h_1(\phi, r) + 1 \, h_2(\phi, r) \qquad (2.5)$$

-6-

Here the fraction $(\nu_1 - 1)/\nu_1$ accounts for the loss of one first generation pion (out of ν_1 initial first generation pions) which is used up in fathering the second generation. In what follows it is convenient to replace the factor in front of h_2 in Eq. (2.5) by $1 \equiv \nu_2/\nu_2$.

Similarly, for the diagram in Figure 3c, in which <u>two</u> of the first generation pions have fathered second generations, the net average distribution is

$$\left\langle \frac{dn}{dr} \right\rangle = \frac{\nu_1 - 2}{\nu_1} h_1(\phi r) + \frac{2\nu_2}{\nu_2} h_2(\phi r) \tag{2.6}$$

Let us now consider a third generation, after which the general treatment of all such diagrams will become clear. A third generation is shown inside the dashed circle in the sample diagram of Figure 3d. If the second generation pion which fathered this third generation of pions happened to have a particular rapidity r_2', then the distribution dn/dr_3 of the pions in the dashed circle is $dn/dr_3 = h_1(r_2', r_3)$. But of course different values of r_2' for the father occur with different frequencies (given by h_2) and it is again most meaningful to speak in terms of an average distribution $\left\langle \dfrac{dn}{dr_3} \right\rangle$ of the pions in the dashed circle,

$$\left\langle \frac{dn}{dr_3} \right\rangle = \frac{\int h_2(\phi, r_2') \, h_1(r_2', r_3) \, dr_2'}{\int h_2(\phi, r_2') \, dr_2' \equiv \nu_2} \equiv h_3(\phi, r_3) \tag{2.7}$$

Also, we can define

$$\nu_3 = \int h_3(\phi, r_3) \, dr_3 \tag{2.8}$$

as the mean multiplicity of pions in a single third generation.

Thus the <u>net</u> average distribution $\left\langle \dfrac{dn}{dr} \right\rangle$ for the (entire) diagram of Figure 3d is just

$$\left\langle\frac{dn}{dr}\right\rangle = \frac{\nu_1^{-2}}{\nu_1} \, h_1(\phi,r) + \frac{2\nu_2^{-1}}{v_2} \, h_2(\phi,r) + \frac{\nu_3}{\nu_3} \, h_3(\phi,r) \tag{2.9}$$

It is by now fairly obvious what the general forms are. The average distribution of a single m^{th} generation of pions is

$$\left\langle\frac{dn}{dr_m}\right\rangle \equiv h_m(\phi,r_m) = \frac{\int h_{m-1}(\phi,r'_{m-1}) \, h_1(r'_{m-1},r_m) \, dr'_{m-1}}{\int h_{m-1}(\phi,r'_{m-1}) \, dr'_{m-1} \equiv \nu_{m-1}} \tag{2.10}$$

and the mean pion multiplicity therein is

$$\nu_m = \int h_m(\phi,r_m) \, dr_m \tag{2.11}$$

The extension of Eqs. (2.5), (2.6), and (2.9) to more complicated explicit graphs is obvious. In all this we have ignored the possibility that energy degradation in the cascade may cause some of the higher generation reactions to deviate from scaling simply because they are not kinematically in the scaling region.

B.   Counting the diagrams

In part A of this section we developed a method — given h_1 — to write down explicitly the net $\left\langle\frac{dn}{dr}\right\rangle$ of pions from any given diagram. It still remains to develop a systematic way of including all possible diagrams and counting over them. This is the subject of this section.

The first thing to notice is that there are many diagrams which give the same contribution in $\left\langle\frac{dn}{dr}\right\rangle$. For example, the diagram in Figure 3e is entirely equivalent to the one in Figure 3b, and the two diagrams in Figure 3f are equivalent to each other. The counting is tremendously simplified if we introduce the notion of a sequence S as being the set of all diagrams equivalent to a given diagram. Individual sequences are identified by subscripts $S_{abc\ldots}$. Here

a is the number of second generations, b is the number of third generations, etc. For example, the two graphs in Figure 3f belong to the sequence S_{22}.

We can write down the $\left\langle \frac{dn}{dr} \right\rangle$ for a representative diagram in a sequence following the procedures outlined in Section IIA. We now ask how many diagrams are contained in a particular sequence. This is simply a problem in combinations. For example, the total number of diagrams in S_{22} is $\binom{\nu_1}{2}\binom{2\nu_2}{2}$ since there are $\binom{\nu_1}{2}$ ways of choosing two pions from the ν_1 first generation pions to father second generations, and there are $\binom{2\nu_2}{2}$ ways of choosing two pions from the $2\nu_2$ pions in the two second generations to father third generations. Therefore, for example, the net contribution of sequence S_{22} is

$$\left\langle \frac{dn}{dr} \right\rangle = \binom{\nu_1}{2}\binom{2\nu_2}{2} \left[\frac{\nu_1 - 2}{\nu_1} \, h_1(\phi, r) + \frac{2\nu_2 - 2}{\nu_2} \, h_2(\phi, r) + \frac{2\nu_3}{\nu_3} \, h_3(\phi, r) \right]$$

$$(2.12)$$

Now we only need to develop a systematic way of counting all the sequences, being sure not to miss any. This is most easily done by introducing $N = 1 + a + b + \ldots$ as the total number of inelastic vertices in a diagram belonging to a particular sequence. (For example, the diagrams in Figure 3f, representing S_{22}, have $N = 5$.) For $N = 1$ there is only one sequence, which we call S_0, the only diagram of which (there is only one since $\binom{\nu_1}{0} = 1$) is shown in Figure 3a; the appropriate $\left\langle \frac{dn}{dr} \right\rangle$ for this sequence is given in Eq. (2.1). For $N = 2$ we again have one sequence, S_1, which contains $\binom{\nu_1}{1}$ diagrams equivalent to Figure 3b, and gives $\binom{\nu_1}{1}$ times Eq. (2.5). For $N = 3$ we have two sequences, S_2 and S_{11}; for $N = 4$ we have S_3, S_{21}, and S_{111}; etc. It was found in practice (after the nuclear physics in Section III was included in the calculation) that sequences beyond $N = 5$ were negligible. (We expect a particular sequence to vanish both as $(\sigma_{in}/\sigma_T)^N$, and because of the improbability of a large number of collisions occurring in a nucleus of finite size. This latter point is discussed in Section IV.

To illustrate our ideas, we shall next present an example in which a particularly simple form for $h_1(\phi,r)$ is chosen.

C. Illustrative Example

The discussion in the introduction regarding Figure 1a indicated that as collision energy increased, the broad pionization region might possibly spread wider and remain flat. Thus at extremely high energies, we expect the salient features of Figure 1a to be reproduced by the idealized multiperipheral-like[3] step function form shown in Figure 1b. In this graph $\left\langle \dfrac{dn}{dr} \right\rangle \equiv h_1(\phi,r)$ is unity from lab rapidity zero (target rapidity) to lab rapidity ϕ (the lab rapidity of the incident pion), and zero elsewhere. The normalization (height) can be adjusted by an overall normalization factor later. Although energy is not conserved in this approximation of $h_1(\phi,r)$, we shall see in Section V that we can handle this essentially minor point.

It is useful for illustrative as well as calculational purposes in the remainder of this paper to assume that multipion production in the inclusive reaction $\pi + p \rightarrow \pi + X$ at high energies is described by this functional form. Thus we take, for the basic diagram of Figure 3a (and Eq. (2.1))

$$h_1(\phi,r) \doteq \Theta(r) - \Theta(r - \phi) \tag{2.13}$$

This assumption results in

$$\nu_1 = \phi \tag{2.14}$$

and in general

$$h_m(\phi,r_m) = \frac{\left(\phi - r_m\right)^{m-1}}{\phi^{m-1}} \tag{2.15}$$

$$\nu_m = \frac{\phi}{m}$$

The first few h_m's are illustrated in Figure 4. It should already be clear that even the simplest cascade, represented by Figure 3b and Eq. (2.5), can result in an average "peaking" at low rapidity, since even a form for h_1 as in Figure 4a — which is the same as Figure 1b — results in a form for h_2 as in Figure 4b, and Eq. (2.5) will look close to a sum of the two curves (4a) + (4b).

III. NUCLEAR PHYSICS

It remains to incorporate some nuclear physics into the discussion of Section II. We shall do this with Glauber theory,[4,5] since it is simple and well understood, and is known to be a good description of particle-nucleus collisions at high energies.

We begin by assuming as usual that the single particle inclusive differential cross section $\dfrac{d\sigma_{inel}}{dr\,dq^2}$ for the process $\pi + p \to \pi + X$ (process I) can be factorized to $h_1(\phi, r)\left[\dfrac{\pi}{p^2}\,|f_{in}(q)|^2\right]$ where ϕ and p are the rapidity and momentum (lab frame) of the incident pion, r and q are the rapidity and transverse momentum of the observed pion, and $f_{in}(q)$ is the transverse scattering amplitude for this inelastic process.

The single particle inclusive differential cross section for the process $\pi + A \to \pi + X$ (process II) on the nucleus A — for a particular sequence $S_{\{\alpha\}}$ having N inelastic vertices (refer also to Figure 2) — can then be written

$$\frac{d\phi}{drd\Delta^2}\Bigg|_{\{\alpha\}} = \frac{1}{4\pi}\begin{pmatrix} A \\ N \end{pmatrix}\int e^{i\vec{\Delta}\cdot(\vec{b}-\vec{b}')}d^2b\, d^2b'\prod_{i=1}^{A}\rho(s_i z_i)\,d^2s_i dz_i$$

$$\left\{\prod_{j=1}^{N}\Gamma_{in}(\vec{b}-\vec{s}_j)\,\Gamma_{in}^*(\vec{b}'-\vec{s}_j)h_1(r_{\alpha_j},r_j)\,dr_j\right\}\frac{dr_0}{\eta_{\{\alpha\}}}$$

$$\delta(r_0-\phi)\left(\sum_{k=1}^{N'}\delta(r_k-r)\right)$$

$$(3.1)$$

$$\prod_{z_a<z_1}\left\langle\left[1-\Gamma_{el}(\vec{b}-\vec{s}_a)\right]\left[1'-\Gamma_{el}^*(\vec{b}'-\vec{s}_a)\right]\right\rangle^1$$

$$\prod_{z_1<z_b<z_2}\left\langle\left[1-\Gamma_{el}(\vec{b}-\vec{s}_b)\right]\left[1-\Gamma_{el}^*(\vec{b}'-\vec{s}_b)\right]\right\rangle^{n_1}$$

$$\prod_{z_2<z_c<z_3}\left\langle\left[1-\Gamma_{el}(\vec{b}-\vec{s}_c)\right]\left[1-\Gamma_{el}^*(\vec{b}'-\vec{s}_c)\right]\right\rangle^{n_2}$$

$$\vdots$$

After we have discussed various terms in this expression, we shall make an approximation which will enable us to rewrite it in much simpler form — see Eq. (3.4).

-12-

Since the main contributions to multiparticle production come from incoherent events, we have applied closure over final nuclear states. Eq. (3.1) is essentially the form obtained in reference 5 for N inelastic scatterings in a nucleus, modified appropriately to handle multiparticle elastic propagation through the nucleus. In this equation, the profile function Γ is the Fourier transform of the transverse part of the scattering amplitude,

$$\Gamma_c(\vec{b}) = \frac{1}{2\pi i p} \int e^{-i\vec{q}\cdot\vec{b}} f_c(\vec{q}) \, d^2q \qquad (3.2)$$

where for convenience we shall work with the usual form

$$f_c(q) = i p Q_c \, e^{-\frac{1}{2} a_c q^2} \qquad (3.3)$$

Here c = "el" or "in" stands for elastic π-p scattering or the inelastic process I above, respectively; $Q_{el} = \frac{1}{4\pi} \sigma_{T_I} \equiv \left(\frac{\sigma_{el} a_{el}}{\pi} \right)^{1/2}$ for a Gaussian amplitude as in Eq. (3.3),

$$Q_{in} = \left(\frac{\sigma_{in} a_{in}}{\pi} \right)^{1/2} \quad ;$$

σ_c and a_c are the (energy-independent) cross sections and widths.

Other features of Eq. (3.1) are as follows. $\vec{\Delta}$ is the transverse momentum transferred to the nucleus. The factor $\binom{A}{N}$ is the number of ways N inelastic collisions can take place among the A nucleons. $\rho(s,z)$ is the single nucleon density within the nucleus, which we shall take to be Gaussian to facilitate calculation: $\rho(s,z) = \rho_0 \exp(-(s^2+z^2)/R^2)$, with R chosen so that the rms radius matches charge form factor data.[6] The N inelastic processes I and the folding of h's for the different generations (as in Section II) is handled in the bracketed product $\left\{ \right\}$ for the sequence $S_{\{\alpha\}}$; $\eta_{\{\alpha\}}$ contains normalizing and counting factors for this sequence. The first delta function guarantees that the incident

pion's rapidity is indeed ϕ; the sum over delta functions guarantees that at least one of the produced pions has the measured rapidity r.

The remainder of Eq. (3.1) treats the elastic scatterings which occur between inelastic collisions. The factor $\Pi_{z_a < z_1}(\ldots)^1$ describes the elastic scattering of the incident pion any number (including zero) of times to the left of the first inelastic vertex at z_1 in Figure 2; z_1 of course is integrated over in the first line of Eq. (3.1). At z_1 the incident particle scatters inelastically (described by the bracketed product $\{\ \}$ mentioned above), producing n_1 first generation particles, which scatter elastically up to the point z_2, as described by the factor $\Pi_{z_1 < z_b < z_2}(\ldots)^{n_1}$ (in Figure 2, $n_1 = 6$). At z_2 another inelastic collision occurs (handled in $\{\ \}$ above), followed by another elastic series, this time for n_2 particles to go from z_2 to z_3 ($n_2 = 8$ in Figure 2). This introduces the factor $\Pi_{z_2 < z_c < z_3}(\ldots)^{n_2}$. We can break these n_2 particles up into those produced at z_2 (which we call second generation) and those produced at z_1 which move past z_2 (which are still first generation). We can obviously go on in this way to build up any chain of cascades in the nucleus that we desire.

(We mention here that the factors $([1 - \Gamma][1 - \Gamma^*])^n$ introduce strong nonclassical effects for large n, such that these terms are damped far less than expected. In the ordinary Glauber theory, where $n = 1$, this effect, due in detail to cross terms in Γ, is $\lesssim 20\%$, whereas in the results we report in the next section we find this effect decreases the damping terms by factors of 10 or more. We have treated this phenomenon in more detail elsewhere.[7])

Eq. (3.1) is still too complicated to handle simply. The fact that inelastic collisions occur at different depths z_i within the nucleus makes treatment of the elastic scattering series very difficult. Therefore we make the "rim approximation," in which we assume that all of the elastic collisions of produced

particles start at the midpoint of the nucleus, z = 0, while the inelastic collisions can occur anywhere. Since this approximation errs in opposite directions for inelastic collisions to the left and right of z = 0, we expect the final result to be insensitive to the approximation. Numerical investigation indicates that this is so.

We can now integrate Eq. (3.1) over Δ to obtain

$$\int d^2\Delta \left.\frac{d\sigma}{drd\Delta^2}\right|_{\{\alpha\}} \sim \left.\frac{dn}{dr}\right|_{\{\alpha\}} \binom{A}{N}\left(\frac{\sigma_{in}}{\pi R^2}\right)^N \left(\frac{R^2}{a_{in}+R^2}\right)^N \int dB^2 e^{-NB^2/(a_{in}+R^2)}$$

$$\left(\sum_{k=0}^{2}\binom{2}{k}\gamma^k \frac{2a_{el}}{2a_{el}+kR^2} \exp\left(-\frac{kB^2}{2a_{el}+kR^2}\right)\right)^{\frac{A-N}{2}} \qquad (3.4)$$

$$\left(\sum_{k=0}^{2n}\binom{2n}{k}\gamma^k \frac{2a_{el}}{2a_{el}+kR^2} \exp\left(-\frac{kB^2}{2a_{el}+kR^2}\right)\right)^{\frac{A-N}{2}}$$

(within an overall constant), where $\gamma = \frac{\sigma_T}{4\pi a_{el}}$. It should be noted that making the rim approximation has enabled us to separate $\left.\int d^2\Delta \frac{d\sigma}{dr\,d\Delta^2}\right|_{\{\alpha\}}$ into an (averaged) factor $\left.\frac{dn}{dr}\right|_{\{\alpha\}}$ pertaining only to the structure of the sequence $\{\alpha\}$ as in Section II, and a factor containing nuclear physics whose only contact with the specific sequence $\{\alpha\}$ is in the numbers N and n.

We can now calculate the net (average) dn/dr for process II; it is

$$\frac{dn}{dr} = \frac{\sum_{\{\alpha\}} \int \left.\frac{d\sigma}{drd\Delta^2}\right|_{\{\alpha\}} d\Delta^2}{\sum_{\{\alpha\}} \sigma_{\{\alpha\}}} \qquad (3.5)$$

Recall also that the sum over sequences $\sum_{\{\alpha\}}$ can be written as $\sum_N \sum_{\{\alpha_N\}}$ where $\{\alpha_N\}$ contains the N-vertex sequences. Here $\sigma_{\{\alpha\}}$ is the production cross section for sequence $S_{\{\alpha\}}$ on the nucleus:

$$\sigma_{\{\alpha\}} = \int \frac{d\sigma}{drd\Delta^2}\bigg|_{\{\alpha\}} drd\Delta^2 \ .$$

Computation of the integral leading to Eq. (3.4) is facilitated by replacing $\vec{b}$ and $\vec{b}'$ of Eq. (3.1)) by $\vec{B} = \frac{\vec{b}+\vec{b}'}{2}$ and $\vec{\beta} = \vec{b}-\vec{b}'$; then the $\vec{\Delta}$ and $\vec{\beta}$ integrals in Eq. (3.5) (and Eq. (3.1)) can be done immediately.

We turn now to a presentation and discussion of results.

IV.　RESULTS

In Figure 5 we show the theoretical particle distributions for a typical emulsion nucleus using the idealized h_1 of Section IIC (Figure 4a) with $\phi = 10$ (which is appropriate in the TeV range), and taking $\sigma_T = 26$ mb and $\sigma_{in} = 22$ mb, and $a_{el} = a_{in} = 9$ $(\text{GeV})^{-2}$. These cross sections are appropriate for pions, which constitute most of the produced particles; but if we used numbers corresponding to incident protons, the results would be indistinguishable from those shown in the figure. As expected, the distribution is quite different from that for an individual nucleon, and shows a marked buildup at small rapidities.

Also shown in Figure 5 are the results of a recent analysis[9,10] of nuclear emulsion data at $E \approx 10^4$ GeV. These were originally used to argue against a flat pionization region. However, it is clear from Figure 5 that the experimental results are actually compatible with a flat pionization region if proper care is taken in handling the nuclear physics, and if the following remarks are noted. The difference between theory and experiment at small rapidities can be

attributed to the facts that (i) in reference 9, low rapidity events were excluded by hand, so the experimental numbers underestimate the true distribution in that region, and (ii) the assumptions that scaling holds to low energies and that energy conservation can be neglected lead to a theoretical overestimate of small rapidity events. In particular, if we assume for illustrative purposes that these assumptions fail at E = 10 GeV, then we can compute the rapidity cutoff. By the definition of rapidity, the upper fraction ξ of a rapidity distribution corresponds to the upper fraction $(1 - e^{-\xi \phi})$ of the corresponding momentum distribution. The upper momentum fraction in our example is $(10^4 - 10)/10^4$, giving for $\phi = 10$ an upper rapidity fraction $\xi \approx .7$ in which our assumptions do not fail. This is the cutoff line shown in Figure 5.

In order to check our method, we have explicitly calculated multiplicities $n = \frac{dn}{dr} dr$ for particle-nucleus interactions and compared the results to experiment. In Figure 6 we show the expected multiplicities from various nuclei, as a function of ϕ, together with the experimental points of reference 11 scaled up by a factor of 3/2 to take rough account of the production of neutrals and then suitably normalized (see first paragraph, Section IIC) to the hydrogen data. We see that the agreement is quite good, a check which gives confidence that other features of intranuclear cascades will be correctly explained by our results. It is also interesting that, according to Figure 6, if the input multiplicity (i.e., on a single nucleon, $n = \int h_1 \, dr$) increases as $\ln(s)$ then the multiplicity on a nuclear target increases faster than $\ln(s)$. (The larger the nuclear target, the faster the multiplicity increases, although the A dependence is relatively weak.)

V. DISCUSSION AND SUMMARY

Although our original MPM distribution in Figure 4a is flat as a function of r, we have seen that the distribution expected from a nucleus is strongly skewed toward small r. The reason for this is quite simple, and has to do with the fact that a particle cannot produce offspring whose energies exceed its own. Thus particles to the right in the chain in Figure 2 will produce lower rapidity offspring, and only the leading particle can produce the highest rapidity.

One important point regarding the skewing of the nuclear distribution should be noted. Although the nucleon and nuclear distributions differ markedly at small r, at large r they are quite similar. Therefore, one way of using these results might be as an indication of when the nuclear effects are important, looking only at high rapidity particles in emulsions. For example, if we wish to work in a region where the effect of the nucleus is less than 10%, we should confine ourselves to the upper 20% of the rapidity plot (see Figure 5). The upper 20% of our rapidity plat in Figure 5 — in which $\phi = 10$ — corresponds to the upper 86% of the longitudinal momentum range. Future experiments could be analyzed in this way, which has the virtue of being largely independent of the nuclear physics.

The discussion in the preceding paragraph, incidentally, shows why the slight energy nonconversation implicit in Eq. (2.13) — Figure 4a — for h_1 is an insignificant problem. In fact, we could replace it with

$$\left\langle \frac{dn}{dr} \right\rangle \equiv h_1(\phi, r) = \Theta(r) - \Theta(r - [\phi - \epsilon])$$

where ϵ is small; this would have the effect of insuring that energy conservation was not violated, and yet the results after folding would be almost indistinguishable from those reported in Section IV, Figures 5 and 6.
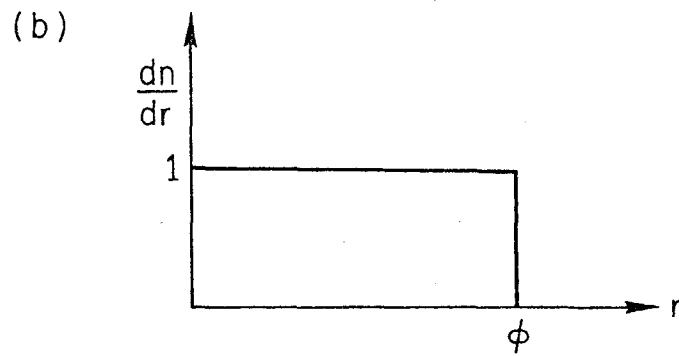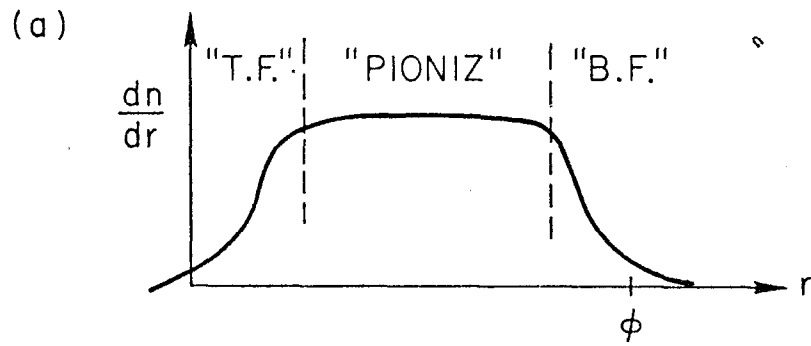
In summary, inclusive cross section experiments on nuclei[12] can provide useful information on the corresponding quantities with nucleon targets. This offers a decided advantage to the experimentalist who wishes to use cosmic rays to study very high energies.

REFERENCES

1. R. P. Feynman, Phys. Rev. Letters $\underline{23}$, 1415 (1969); J. Beneke,

    T. T. Chou, C. N. Yang, and E. Yen, Phys. Rev. $\underline{188}$, 2159 (1969).

2. P. M. Fishbane, J. L. Newmeyer, and J. S. Trefil, Phys. Rev. Letters

    $\underline{29}$, 685 (1972).

3. K. A. Ter-Martirosyan, Nucl. Phys. $\underline{68}$, 591 (1965); see also

    F. Zachariasen and G. Zweig, Phys. Rev. $\underline{160}$, 1322 (1967).

4. R. J. Glauber in High Energy Physics and Nuclear Structure, ed.

    G. Alexander (North Holland, Amsterdam, 1967), p. 311 et seq.

5. J. S. Trefil and F. von Hippel, Phys. Rev. (to be published), and

    references contained therein.

6. R. Herman and R. Hofstadter, "High Energy Electron Scattering Tables,"

    Stanford U. Press, Stanford, California (1960).

7. P. M. Fishbane, J. L. Newmeyer, and J. S. Trefil, Phys. Letters

    (to be published).

8. J. S. Trefil, Phys. Rev. $\underline{D3}$, 1615 (1971).

9. L. von Lindern, R. S. Panvini, J. Hanlon, and E. O. Salant, Phys. Rev.

    Letters $\underline{27}$, 1745 (1971).

10. For a different treatment of this data, see A. Krzywicki and B. Petersson,

    Phys. Rev. $\underline{D6}$, 924 (1972).

11. L. W. Jones, A. E. Bussian, G. D. DeMeester, B. W. Loo,

    D. E. Lyon, Jr., P. V. Ramana Murthy, R. F. Roth, J. G. Learned,

    F. E. Mills, D. O. Reeder, K. N. Erickson, and B. Cork, Phys. Rev.

    Letters $\underline{25}$, 1679 (1970).

12. See also P. L. Jain and Z. Ahmad, Phys. Rev. Letters $\underline{28}$, 459 (1972).
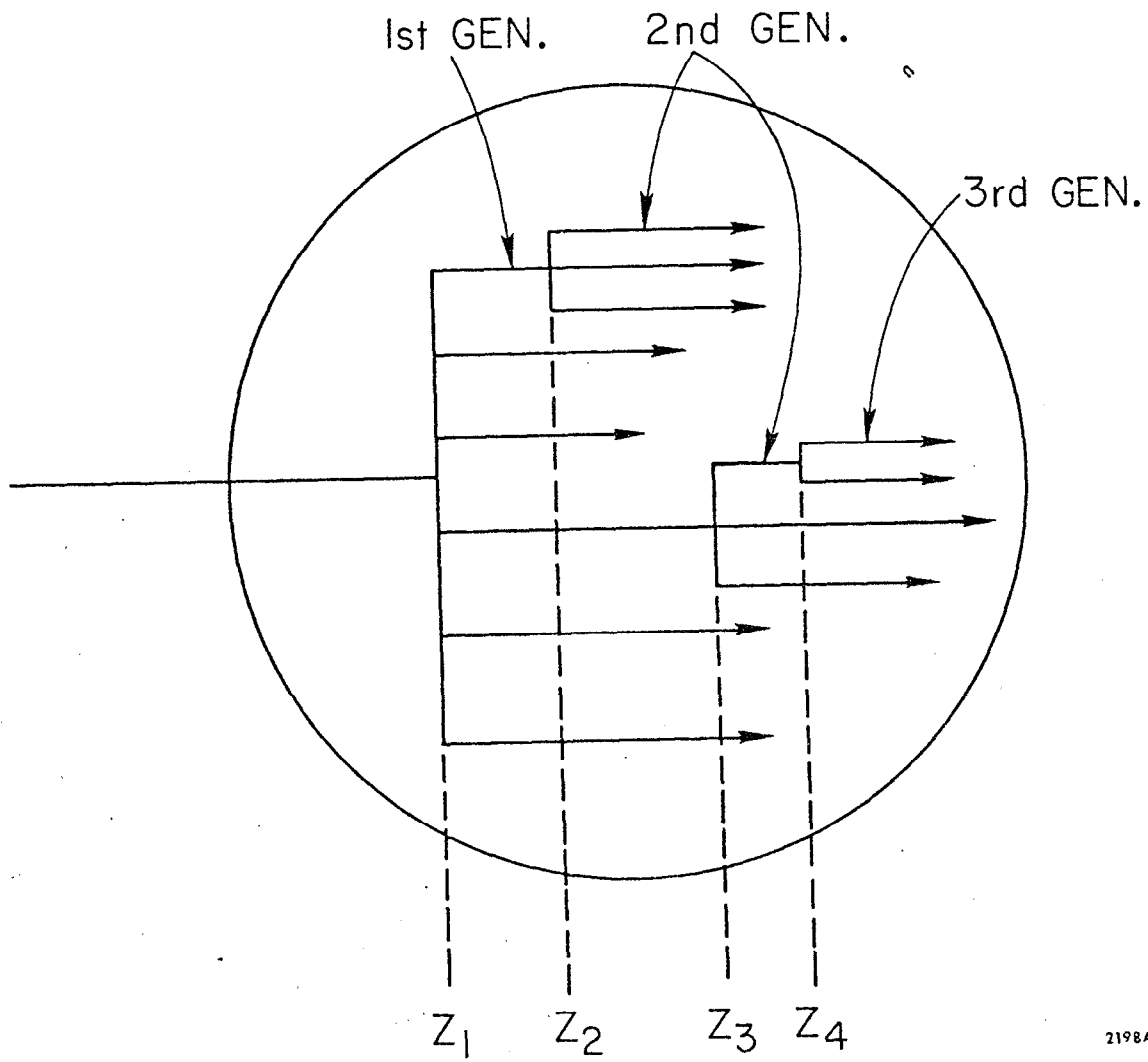
FIGURE CAPTIONS

1. a.   A single particle inclusive distribution $\frac{dn}{dr} \equiv h_1(\phi, r)$ (schematic)

    showing the breakup into target fragmentation, pionization, and beam

    fragmentation regions.

    b.   Idealized form for $h_1(\phi, r)$ used to simplify calculation in Section 2C.

2. A typical intranuclear cascade.

3. Various individual cascade diagrams. See text (Section II) for discussion.

4. The first three component distributions $h_m(\phi, r)$ (m = 1, 2, 3) given the step

    function form (2.13) for $h_1(\phi r)$. (See Fig. 1b.)

5. The solid line in this figure illustrates the theoretical single particle

    inclusive buildup at lower rapidities due to intranuclear cascading. The

    nucleus is ^{80}Br, and the incident proton's rapidity was taken as $\phi = 10$,

    corresponding to ~ 20 GeV. Shown as a dashed line is the step function

    distribution assumed for $p + {}^1H \rightarrow \pi + X$. The data of Ref. 3 is normalized

    and superimposed. The disagreement of theory and experiment at low r is

    discussed in the text.

6. The solid lines represent pion multiplicities on ^1H, ^{12}C, and ^{208}Pb as a

    function of incident pion rapidity, using the single particle distribution

    discussed in the text. The experimental points for ^1H and ^{12}C are from

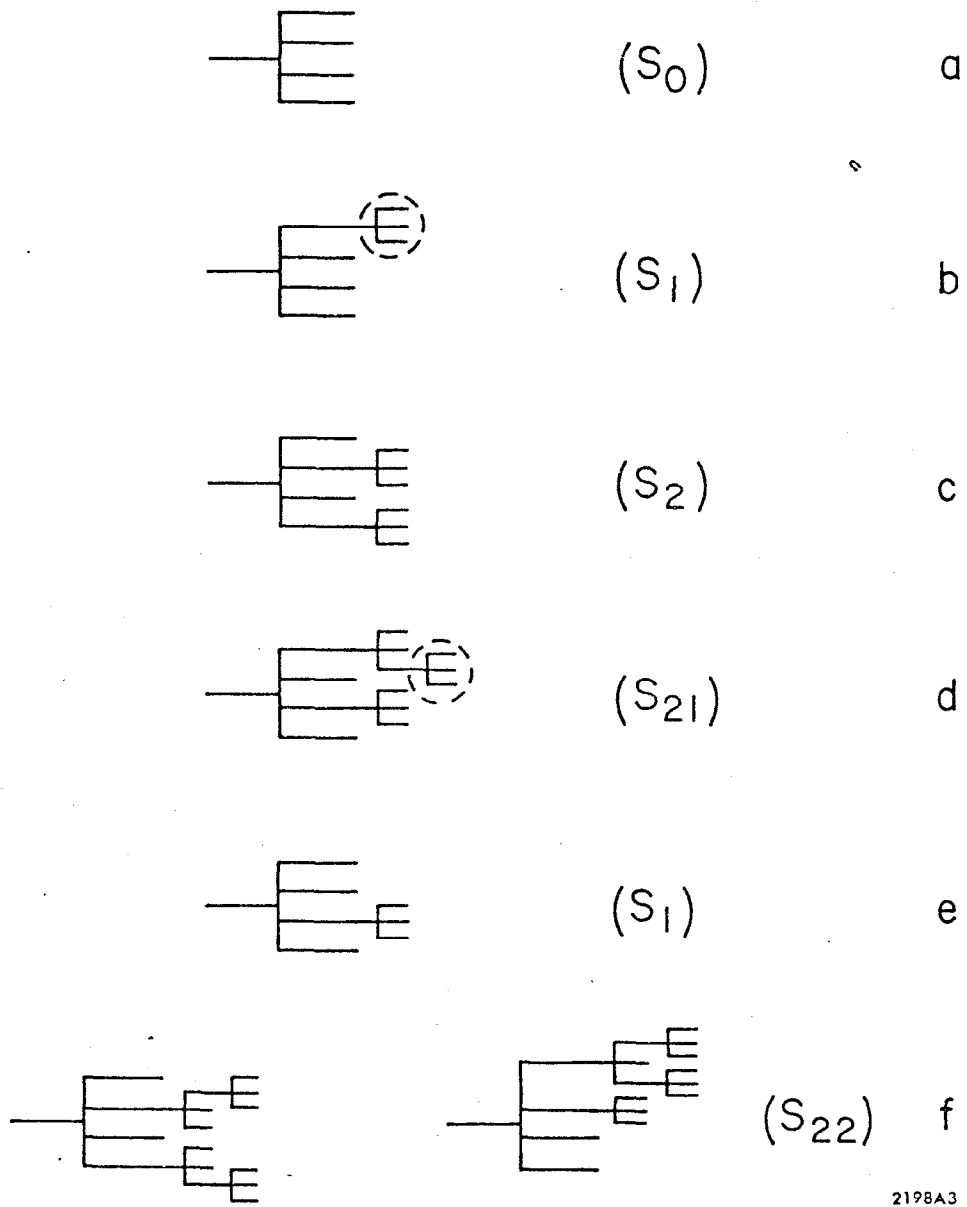   Ref. 10, normalized to match the theory at the 200 GeV (lowest point)
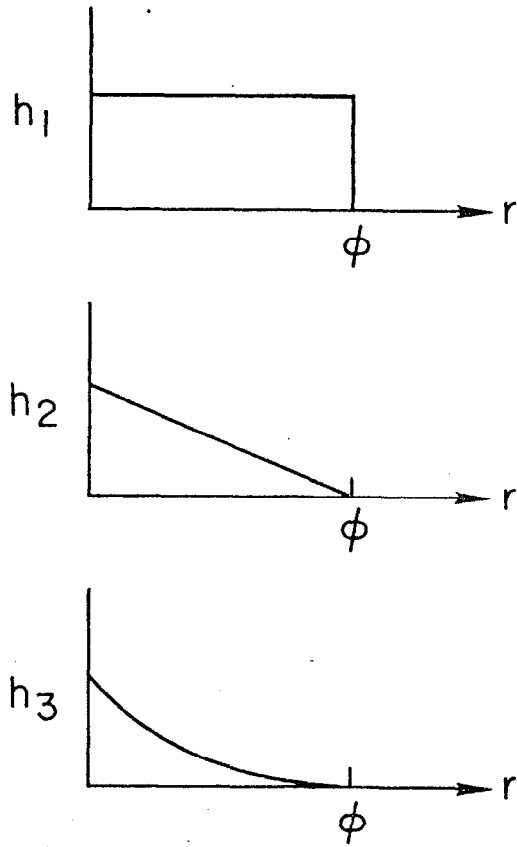
    hydrogen point.

Fig. 1

Fig. 2

(S_0) a

(S_1) b

(S_2) c

(S_{21}) d

(S_1) e

(S_{22}) f

2198A3

Fig. 3

Fig. 4

2198A2

Fig. 5

Fig. 6

2198A6